Nanoscience and Nanotechnology Letters
Vol. 7, 743–748, 2015

Fabrication and Characterization of the AZO/Ag/AZO Transparent Conductive Films Prepared by RF Magnetron Sputtering Using Powder Targets

Liu Si-Ning, Zhou Yan-Wen*, Sha Tian-Yi, and Wu Fa-Yu

School of Materials and Metallurgy, University of Science and Technology Liaoning, No. 185 High-Tech District, AnShan, Liaoning, 114051, China

The sandwich films composed of aluminum ions doped zinc oxide (AZO)/silver (Ag)/aluminum doped zinc oxide (AZO) films were prepared by RF magnetron sputtering using the powder targets at room temperature. The morphology and crystallinity, as well as the optical and electrical properties of the as-synthesized films were examined by using different characterization equipments, including X-ray diffraction, Atomic force microscopy, UV-visible spectrophotometer and the Hall-effect measurement. The XRD patterns indicate the existence of the polycrystalline structure with the preferred orientations of ZnO (002) and Ag (111). The AZO/Ag/AZO films have dense columnar structures according to the images captured by the atomic force microscopy. The transmittance of the film at 550 nm is ~85% reflected in the UV-visible spectra. The charge carrier concentration and mobility, the resistivity and the sheet resistance of the tri-layer film is about $3.6 \times 10^{22}/cm^3$, 9.0 cm^2/Vs, 1.9×10^{-5} $\Omega \cdot cm$, and 2.6 Ω/sq, respectively. The AZO/Ag/AZO film has great promises in the industrial applications as transparent electrodes.

Keywords: TCO Multilayer Films, Metal Matrix TCO Films, Powder Target, RF Magnetron Sputtering.

1. INTRODUCTION

Transparent conductive oxide (TCO) films, which can be used as both window and conductive layer in optoelectronic, electrical devices and photovoltaics, become incredibly significant to improve the performance of these devices, as well as to reduce the cost and weight of these devices. Tin doped indium oxide (ITO) is considered to be the most suitable material as one of the transparent conductive electrodes due to its low electrical resistivity ($\sim 2.5 \times 10^{-4}$ $\Omega \cdot cm$) at relatively high transmittance.[1–3] The synthesis of ITO nanowire used as a photo anode in dye-sensitized solar cells has been studied, and nanowire ITO was recommended to take over the wide band gap conductive nanowires, such as TiO_2.[4,5] However, the scarcity of indium in the earth results in the high price and limits the practical applications of ITO in certain areas. Therefore, it is urgent to find new TCO materials with the transmittance and electrical conductivity comparable to those of ITO to replace ITO in industrial applications. Although tremendous progress has been made on doped TCOs, TCO materials with their bulk carrier concentrations comparable to ITO (up to 10^{21} cm^{-3}) are still not available.[1–3]

The high conductivity and transmittance of the metal matrix tri-layer TCO films have attracted intensive studies in recent years. For instance, SiKai Zhang et al. reported that the ZnO/Au/ZnO films, prepared by MOCVD and RF magnetron sputtering, were with the transmittance up to 75.3% and resistivity of 2.7×10^{-3} $\Omega \cdot cm$.[6] A transmittance of 84% and a resistivity of 7.92×10^{-5} $\Omega \cdot cm$ have been achieved in the AZO/Cu/AZO film prepared by RF magnetron sputtering and ion plating.[7] The studies on ITO/Ni/AZO and AZO/Ni/AZO tri-layer films demonstrated that a layer of 5 nm Ni metal film enhanced the electrical and optical properties due to the quantum efficiencies.[8–10] The studies on the ITO/Ag/ITO and $SnO_2/Ag/SnO_2$ films showed that the optical and electrical properties of the metal matrix tri-layer films beard better transmittance and conductivities than those of ITO and AZO films.[11–13] The metal layers ensure the conductivity in these metal matrix tri-layer films, while the high refractive index of TCO layers guarantee the transmittance within the visible light due to their anti-reflection effect.

The nanowire metal matrix films have great potentials as transparent conductors. Zeng et al.[14] have reported that the films composed of Ag nanowire buried in polyvinyl alcohol (AgNW-PVA), had an optical transmission of 87.5%

*Author to whom correspondence should be addressed.

(at 550 nm) and a sheet resistance of 63 Ω/sq, which were very close to the optoelectronic requirements for touch screen panels. Graphene with a sheet resistance of 310 Ω/sq at a transmittance of 90% has been considered to be another promising candidate as transparent conductor. To further reduce of the sheet resistance, hierarchical structures composed of graphene/Ag grid films with the optical and electrical properties of 94% transmission with a sheet resistance of 0.6 Ω/sq were designed.[15] Also, the transparent composite electrodes based on Ag nanowires on metal oxide films showed the promising a transmittance of 93.4% (at 550 nm) and a resistivity of 11.3 Ω/sq.[16]

Magnetron Sputtering is one of the most popular techniques to prepare TCO films. The effect of the magnetron sputtering parameters on the structure and the performance of the Ag based tri-layer TCO films had been studied.[17–19] Ceramic or metal targets were used in most of the sputtering processes. The manufacture procedures of those solid targets are complex, and normally expensive. Additionally, the ceramic targets are easy to crack because they are fragile during the sputtering process. To control the position of the target, a special optical emission monitor installed in the sputtering rig is needed during the reactive sputtering. Wendt and Ellmer et al. reported that the oxygen pressure was a tricky parameter and the as-deposited TCO films obtained by reactive sputtering had to be annealed to further improve the performance.[20–22] The thermal expansion coefficient of Ag is much larger than those of TCO films. The structure of Ag films might become loose during the sputtering, and Ag was easy to be oxidized during the temperature raise. Again, the ever-demanding needs of plastic substrates in flexible electronics require a fabrication process at low temperatures.[23,24] Taken together, the use of metal targets to proceed the reactive sputtering should be avoided when prepare the metal matrix tri-layer TCO films.

Among metals, Ag is considered to be the one with the lowest absorbance in the visible wavelength range and the lowest reflection within the infrared wavelength range, the highest conductivity, making it suitable to be used as the metal layer in these TCO/metal/TCO films.[2,25] AZO is considered to be a promising substitute of ITO, owing to its low cost, non-pollution, wide optical bandgap (3.3 eV), high transparency, good conductivity, and chemical and heat stabilities. The studies by Ando et al. showed that the AZO/Ag/AZO films were with high transparency and good conductivity, as well as the anti-surge capacity.[26,27]

Taken together, in this study, AZO and Ag were selected to prepare the AZO/Ag/AZO films by RF magnetron sputtering at room temperature. The AZO films were deposited using the mixed alumina and zinc oxide powder as a target. Ag plate target was used to create the Ag film. The glass slides were used as the substrate for supporting the AZO/Ag/AZO tri-layer films. The loosely pressed oxide powder target avoided the cracking of the ceramic solid targets. Also, it is not necessary to use oxygen as the reactive gas by employing the oxide target. Further, the adoption of the oxide target could protect the Ag layer from oxidization. No post-annealing treatment was applied to the as-deposited AZO/Ag/AZO film, allowing for the protection of the structure of the Ag layer. The electrons in the plasma created during the RF process travelled forward and back, greatly improved the conductivity of the oxide target and ensured the sputtering efficiency.

2. EXPERIMENTAL DETAILS

2.1. Design of the Film Thicknesses

When the thicknesses of Ag films are less than 10 nm, it usually led to the formation of discontinuous structures with numerous isolated islands, resulting in poor conductivities of the films.[2,16] While when the thicknesses of Ag films is over 20 nm, the transmittance became extremely low in the UV and visible wavelength range.[3,28,29] Considering the above discussions, the thickness of the Ag layer in this experiment was selected to be 14 nm.

Based on the film interference theory, the reflection loss of the light is prevented and the transmittance is increased as the path length of the reflection light is equal to half of the wavelength of the incident light in the medium, causing the occurrence of the distractive interference. Therefore, the thickness of the AZO films without the Ag layer was designed to be 1/4 of the incident wavelength in the AZO films. The thicknesses of the AZO layers were estimated to be 18–60 nm, according to the following formula: $\Delta = 1/2(2k+1)\lambda$, where '$k$' presents the extinction coefficient, and 'λ' is the wavelength of the incident light. Also, the refractive indexes of AZO and Ag films were carefully considered during the calculation.[3,28] The thickness of the AZO film in the experiment was set to be 30 nm. Firstly, a 30 nm of AZO layer was deposited on the glass slide, then a 14 nm of Ag layer was deposited onto the AZO matrix. At last, another 30 nm of AZO layer was prepared on top of the Ag matrix again. The sandwich structure of the AZO/Ag/AZO films was finally obtained.

2.2. Procedure

The AZO/Ag/AZO films were deposited in a powder rig by RF magnetron sputtering. The target in the powder rig is located at the bottom of the chamber and faced up. The powder blends were made by mixing an appropriate amount of zinc oxide and aluminum oxide powders in 99.99% purity in a rotating drum for several hours. The batches were produced with a 2 at% dopant concentration. Following the blending, approximately 100 g of the powder was evenly distributed across the surface of a copper backing plate on the magnetron to form the sputtering target. The backing plate had been recessed to a depth of 2 mm to allow the creation of a reasonable target thickness. The powder was lightly tamped down to produce a smooth target surface with a uniform thickness. No further

Table I. Deposition parameters and the thickness of the films.

Film	Power, W	Thickness, nm
AZO	125	30
Ag	100	14
AZO/Ag/AZO	125/100/125	30/14/30

treatment was involved in target production. The solid Ag target with a purity of 99.999% was used to deposit the Ag layer. SAIL 7101 glass slides were used as the substrate, which was ultrasonically cleaned by ethyl alcohol, rinsed by ionized water, dried by nitrogen before being fixed into the vacuum chamber. The rig was then pumped down to 3.0×10^{-3} Pa and refilled with 99.99% of argon (Ar) untill the chamber pressure is up to 0.3 Pa. The deposition parameters of the films were sumarrized in Table I.

2.3. Characterization

The crystallinity of the coatings was investigated using an X'Pert Pro X-ray diffractometer (XRD), operating in the small angle diffraction mode with Cu kα radiation created at 40 kV voltage. The scanning angle was set from 20 to 80 degree. The diffraction peaks were analyzed using the Highscore plus software considering the angle positions, intensities and full width half maximum (FWHM). The morphology of the films was characterized using a CSPM5500 Atomic force microscopy (AFM) operated in a tapping mode at 2 Hz. The scanning range was within 7000 nm. Then imager 4.6 software was applied to analyze the particle size and the roughness of the films. The thickness of the films was measured by Alpha-step D-100. The optical property in the range of 300∼800 nm was detected by a Lambda 900 UV Vis spectrophotometer. The electrical property of the films was test by the Hall Effect 8800 measurement.

3. RESULTS AND DISCUSSION

3.1. Crystal Structure

Figure 1 shows the XRD patterns of the as-deposited AZO, Ag and AZO/Ag/AZO films. Compared to the standard PDF card (No. 36-1451), (002) and (101) diffraction peaks appeared in the AZO film deposited on the glass substrate, corresponding to the wurtzite ZnO, as shown in Figure 1(a). The strong preferred (002) orientation is associated with its *C* axis, which is the growth direction with the lowest Gibbs free energy. After the Al^{3+} dopant being added, no additional peaks emerged, indicating that the aluminum ions are not existing as crystalline byproducts, but most probably substituted the position of the Zn^{2+} ions. The XRD spectrum of the Ag film on the glass substrate is shown in Figure 1(b). The (111), (200), (220) and (311) diffraction peaks imply the formation of the face-centered cubic Ag structure, in accordance with the standard Ag PDF card (No. 01-087-0718). The polycrystalline structure of the Ag promotes the continuity of the Ag film.

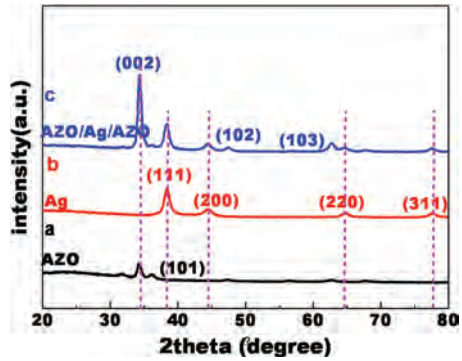

Fig. 1. XRD patterns of the (a) AZO/glass, (b) Ag/glass and (c) AZO/Ag/AZO films.

Figure 1(c) shows the XRD pattern of the AZO/Ag/AZO film, where the main diffraction peaks of (002) ZnO and (111) Ag can be seen.

The standard (002) diffraction of ZnO is positioned at 34.4°. The ZnO (002) diffraction peak appeared at 34.19° within the AZO/glass and at 34.36° for the AZO/Ag/AZO films, which are lower than that of the standard value (Table II). Also, the intensity of the top AZO (002) diffraction peak was much stronger than the one from the AZO/glass film. E. Ando, et al. has revealed that the existence of the compressive internal stress in the films resulted in the shift of the ZnO (002) peak to the low diffraction angle side.[27] Therefore, the Ag/AZO matrix promoted the crystallinity of the top AZO layer and released the compressive internal stress.

Compared to the standard 2theta angle of Ag (111) (at 38.2°), the Ag film on the glass substrate showed a high diffraction angle, which indicated the tensile internal stress in the film. The residue tensile internal stress in the film is not preferred as the film is tend to be peeled off from the glass substrate.[30] The (111) peak of the Ag layer between the two AZO layers moved to the low diffraction angle direction and was lower than that of the standard Ag (111). The compressive stress existed in the tri-layer film allow for the adhesion among the tri-layers and to the glass substrate.

The grain size can be evaluated by the Scherrer formula, $L = 0.9\lambda/(\beta_g \cos\theta)$, where '$L$' represents crystal

Table II. Analysis of ZnO (002) and Ag (111) on different substrates.

Main peaks	Position [°2Th.]	Height [cts]	FWHM [°2Th.]	Standard Position [°2Th.]
(002) AZO/glass	34.19	806	0.49	34.4 [36-1451]
(002) AZO/Ag/AZO	34.36	4265	0.54	
(111) Ag/glass	38.42	1538	0.49	38.2 [01-087-0718]
(111) AZO/Ag/AZO	38.15	1260	0.34	

grain size, 'λ' is the X-ray wavelength and 'θ' is the diffraction angle. Also, 'β_g', broaden parameter of the diffraction peak, can be represented by the full width of maximum height (FWHM) of the peak. Therefore, the FWHM can be used to evaluate the grain size. For example, a small (broad) FWHM means a large (small) grain size. In Table II, it is interesting to notice that the FWHMs of the ZnO (002) and the Ag (111) on the amorphous glass substrate were the same. While the FWHM of Ag (111) diffraction peak on the crystallized AZO became small. The diffraction peak of AZO on Ag/AZO is large. Therefore, the grain size of the films was highly dependent on the composition and structure of the substrate. The similar grain size of Ag and AZO on glass might be due to the amorphous structure of the glass substrate. The crystallized matrix can facilitate the growth of the crystals compared with the amorphous substrate. Therefore, the grain size of the Ag film on the AZO matrix was larger than that of the Ag film on glass. The lattice constants of Ag and ZnO are 0.408 nm and 0.325 nm, respectively. It might be due to the requirement of the lattice matching between Ag and AZO makes the crystal size of AZO layer on the Ag matrix small.

3.2. Morphology Structure

The morphologies and the sizes of the AZO/glass, Ag/AZO and AZO/Ag/AZO films were characterized by AFM observations. As can be seen in Figure 2, the coatings have dense columnar structures and appear to be defect-free, grown perpendicularly to the glass substrate along *C* axis. The roughness, the particle size and tcolhe umnar depth of the films were analyzed by Imager 4.6 software installed in AFM CSPM5500 (see Table III).

Based on Figure 2(a), the morphology of the AZO on the glass substrate exhibited slender grains with a smooth and dense surface. There might be two possible reasons to form the fine grains for the AZO on glass:

(1) the amorphous structure;
(2) the ultra-thin thickness.

Different to the AZO grown on glass, the growth of the Ag film shown in Figure 2(b) was directly on the crystallized AZO matrix. It was easy to form slightly large columns and grains of Ag than the AZO/glass film. The increase of the Ag grain size is consistent with the XRD results demonstrated in Figure 1 and Table II. The morphology of the AZO layer on the Ag/AZO matrix is shown in Figure 2(c), in which the grain size and the columns became even larger than those within the crystallized Ag

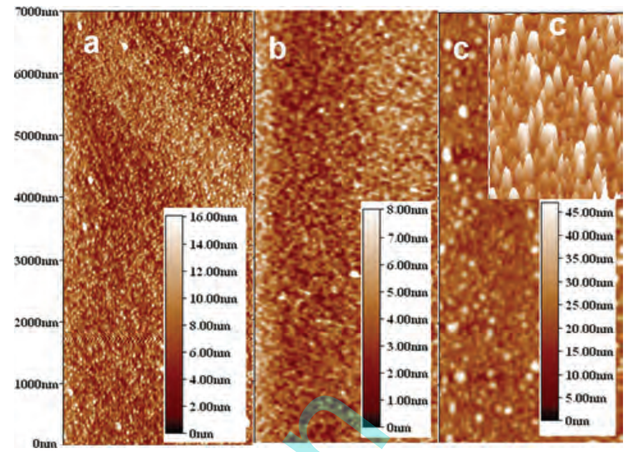

Fig. 2. AFM images of the films: (a) AZO/glass, (b) Ag/AZO and (c) AZO/Ag/AZO.

layer. Also, the depth bar of the Ag layer was only 8 nm, which was much less than those of AZO on glass and AZO on Ag/AZO matrix, as shown in Figure 2. The reason might be the thickness of the Ag layer was extremely thin (only 14 nm). As the thickness increases, the depth of the AZO layer on the Ag/AZO was the stacking of the three layers (equal to 45 nm). The roughness is normally related to the depth of the film. The depth of the Ag layer was the shallowest, rendering a smooth surface of the film. The experimental results proved the conclusions above discussed. For instance, the AZO matrix can assist the formation of continuous Ag films.

3.3. Optical Property

Figure 3 shows the transmittance spectra of the AZO/glass, the Ag/glass and the AZO/Ag/AZO films. The transmittance of the 30 nm AZO/glass, 14 nm Ag/glass and AZO/Ag/AZO/glass are 95.8%, 56.8% and 85% at the wavelength of 550 nm, respectively. The optical band gap of the AZO is calculated to be about 3.3 eV, which is much larger than the energies of the photons of the visible light, making the light can penetrate through the AZO film.

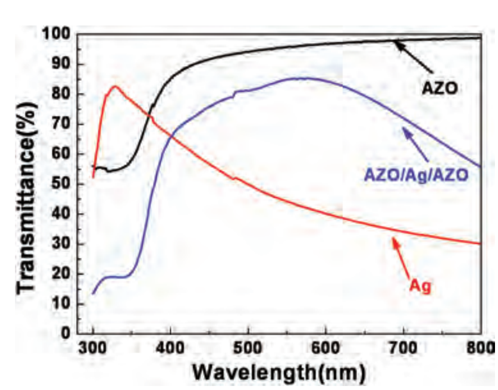

Fig. 3. Transmittance spectra of the AZO/glass, Ag/glass and AZO/Ag/AZO films.

Table III. Summaries of the grain size within different films.

Film	Roughness, nm	Diameter, nm	Depth, nm
AZO/Glass	1.89	58	3.87
Ag/AZO	0.86	107.9	1.78
AZO/Ag/AZO	3.5	132.9	6.34

On the other hand, the absorption of the Ag film within visible wavelength range is quite high due to its metal property. The transmittance of the Ag film is getting low as the wavelength of the light increases. The AZO/Ag/AZO sandwich film was designed in this experiment to improve the transmittance of the Ag film. The depression of the interference of the incident and reflected lights occurs when the optical path difference of the reflected light (Δ) is half of the wavelength of the incident light, i.e., $\Delta = 1/2(2k+1)\lambda$. The condition of $\Delta = 1/2(2k+1)\lambda$ is satisfied if the thickness of the films is set to be $1/4\lambda$, in which 'k' and 'λ' represent the extinction coefficient and the wavelength of the incident light in the film media, respectively. The anti-reflective effect is obvious due to the deductive interference.[31–33] In this study, the thickness of the AZO films is selected to be 30 nm, which is effective to weaken the reflection of the visible light (with anti-reflective properties). The transmittance of the AZO/Ag/AZO film was improved up to 85% compared to that of 56% of the Ag film.

3.4. Electrical Property

Detailed studies of the influence of the structure of the single layer and tri-layer films on the electrical properties are also carried out. The results are summarized in Table IV. The 30 nm AZO film prepared on the amorphous glass substrate was ultra-thin. The grain size in the AZO film was very small, as reflected by the low and wide X-ray diffraction peaks in Figure 1(a) and the slender columnar structure in Figure 2(a). The mobility of the charge carriers in the AZO/glass film was very low (down to 0.16 $cm^2/V \cdot s$). The study on the structure of the 14 nm Ag/glass film proves the continuous nature with an excellent crystallinity (see Fig. 1(b)). The crystallinity of the Ag film is favorable for the movement of the charge carriers within the film. Combined with the metallic property of the Ag film, the sheet resistance, resistivity, the charge carriers' concentration and the mobility of the Ag/glass film are as low as 5.56 Ω/sq, 7.78×10^{-6} $\Omega \cdot cm$, and 5.35 $cm^2/V \cdot s$, respectively, while the concentration of the charge carriers can reach as high as $1.51 \times 10^{+23}/cm^3$. The parallel resistance of the metal matrix films is equivalent to a single resistor, i.e., $1/R_s = 1/R_s(AZO) + 1/R_s(Ag) + 1/R_s(AZO)$. It can be predicted that the sheet resistance of the AZO/Ag/AZO tri-layer film is dominated by the Ag layer. It is true that the AZO/Ag/AZO film is an n-type semi-conductor with a very good electrical property with the electrons as the charge carriers. The sheet resistance, the resistivity, the carriers' concentration and the mobility of the tri-layer film is 2.62 Ω/sq, 1.94×10^{-5} $\Omega \cdot cm$, $3.60 \times 10^{+22}/cm^3$ and 8.95 $cm^2/V \cdot s$, respectively.

Table IV. Electrical properties the AZO, Ag and AZO/Ag/AZO films.

Film	Thickness, nm	Resistance, Ω/sq	Resistivity, $\Omega \cdot cm$	Carriers' concentration, cm^{-3}	Carriers' mobility, $cm^2/V \cdot s$
AZO/glass	30	$1.55 \times 10^{+5}$	4.65×10^{-1}	$8.67 \times 10^{+19}$	0.155
Ag/glass	14	$5.56 \times 10^{+0}$	7.78×10^{-6}	$1.51 \times 10^{+23}$	5.35
AZO/Ag/AZO	74	$2.62 \times 10^{+0}$	1.94×10^{-5}	$3.60 \times 10^{+22}$	8.95

The *resistivity* is the reciprocal of the conductivity, which is defined as the longitudinal electrical resistance of a uniform rod with a unit length and a unit cross-sectional area, widely used as the basic parameter of the conductive property of a semi-conductive material with a unit of ohm-cm. Resistivity is independent on the shape and size of the material. *Sheet resistance* represents the resistance between two sides of a square, which is independent on the area of the square if the area is much larger than the thickness of the thin film, but is related to the thickness of the film. The relationship between the resistivity and the sheet resistance is: $R_s = (\rho/d) = (4.53V/I)$, where '$V$' and '$I$' are the hall voltage and the current, respectively. 'd' stands for the thickness of the film. The sheet resistance is dependent on the thickness of the film. The thickness of the tri-layer film was the sum of the thicknesses of the three layers, which is 74 nm and much thicker than that of the Ag/glass (14 nm). Therefore, the sheet resistance of the AZO/Ag/AZO decreased when compared with that of the Ag/glass film. Resistivity is determined by the sheet resistance and the thickness of the film. Considering the tri-layer film as a whole, it is understandable that the resistivity of the tri-layer film increased due to the relatively poor conductivity of the AZO.

As discussed above (Fig. 1 and Table II), the crystallinity of the Ag layer is promoted by the crystalline AZO matrix. The improvement of the crystallinity may reduce the electron scattering from the grain boundaries, resulting in the increase of the electrons' mobility within the Ag layer. Also, the growth of the grains within the AZO layer on the Ag/AZO matrix promotes the mobility of the charge carriers. Therefore, it can be seen from Table IV, the carriers' mobility in the tri-layer AZO/Ag/AZO film was larger than those in the AZO and the Ag films prepared on glass, although the interface between the adjacent layers might block the movement of electrons.

Again, the bulk concentration of the tri-layer film should compose the two AZO layers and the Ag layer. Therefore, it is one order lower than that of the single Ag film.

In general, this ultra-thin (~74 nm) AZO/Ag/AZO tri-layer film has a transmittance of 85% at the wavelength of 550 nm, and with a sheet resistance of only 2.62 Ω/sq. The optical and the electrical properties of the metallic matrix film can meet the requirements of most of the optoelectronic devices and solar cells acting as both the window and the electrode layer. The AZO/Ag/AZO film has demonstrated great potentials as a new TCO film with the possibility to substitute industrially used ITO.

4. CONCLUSIONS

The AZO/Ag/AZO tri-layer TCO film prepared by RF magnetron sputtering using the powder target at room temperature shows very good electrical conductivity and high light transmittance. The sheet resistance, the resistivity, the bulk carriers' concentration and mobility, and the transmittance is 2.62 Ω/sq, 1.9×10^{-5} Ω · cm, 3.6×10^{22}/cm^3 and 8.95 cm^2/V · s, and 85% at the wavelength of 550 nm, respectively. The ultra-thin metal matrix TCO film can be prepared at a low cost, bearing great promise in replaying of the commercially used ITO films.

Acknowledgments: The authors would like to thank NSFC (Nos. 51172101 and 51372109) and LNET (LR2012009) for funding this research.

References and Notes

1. J. R. Bellingham, W. A. Phillips, and C. J. Adkins, *J. Mater. Sci. Lett.* 11, 263 (**1992**).
2. Z. Wang and X. Cai, *J. Funct. Mater.* 35/s1, 79 (**2004**).
3. X. Cai, *J. Funct. Mater.* 38/s1, 1 (**2007**).
4. L. Li, S. Chen, J. Kim, C. Xu, Y. Zhao, and K. J. Ziegler, *J. Cryst. Growth* 413, 31 (**2015**).
5. L. Li, C. Xu, Y. Zhao, S. Chen, and K. J. Ziegler, *ACS Appl. Mater. Interfaces* 7, 12824 (**2015**).
6. S. K. Zhang, B. L. Zhang, and Z. F. Shi, *Chin. J. Luminescence* 33, 934 (**2012**).
7. S. Song, T. Yang, M. Lv, Y. Li, Y. Xin, L. Jiang, Z. Wu, and S. Han, *Vacuum* 85, 39 (**2010**).
8. M. M. D. Kumar, S. M. Baek, and J. Kim, *Mater. Lett.* 137/0, 132 (**2014**).
9. M. M. D. Kumar, H. Kim, Y. C. Park, and J. Kim, *Mater. Sci. Engi.: B* 195, 84 (**2015**).
10. J.-H. Yun, N. Duraisamy, M. M. D. Kumar, and J. Kim, *Mater. Lett.* 143, 215 (**2015**).
11. K. H. Choi, J. Y. Kim, Y. S. Lee, and H. J. Kim, *Thin Solid Films* 341, 152 (**1999**).
12. S. Yu, W. Zhang, L. Li, D. Xu, H. Dong, and Y. Jin, *Thin Solid Films* 552, 150 (**2014**).
13. S. H. Yu, C. H. Jia, H. W. Zheng, L. H. Ding, and W. F. Zhang, *Mater. Lett.* 85, 68 (**2012**).
14. X.-Y. Zeng, Q.-K. Zhang, R.-M. Yu, and C.-Z. Lu, *Adv. Mater.* 22, 4484 (**2010**).
15. T. Gao, Z. Li, P.-S. Huang, G. J. Shenoy, D. Parobek, S. Tan, J.-K. Lee, H. Liu, and P. W. Leu, *ACS Nano* 9, 5440 (**2015**).
16. A. Kim, Y. Won, K. Woo, S. Jeong, and J. Moon, *Adv. Funct. Mater.* 24, 2462 (**2014**).
17. F. Jia, X. L. Qiao, and J. G. Chen, *Opto-Electron. Eng.* 34, 38 (**2007**).
18. J. Li, J. L. Yan, and C. X. Yang, *Electron. Components Mater* 26, 52 (**2007**).
19. F. Li, Y. Zhang, C. Wu, Z. Lin, B. Zhang, and T. Guo, *Vacuum* 86, 1895 (**2012**).
20. K. Ellmer and R. Wendt, *Surf. Coat. Technol.* 93, 21 (**1997**).
21. R. Wendt and K. Ellmer, *Surf. Coat. Technol.* 93, 27 (**1997**).
22. K. Ellmer, F. Kudella, R. Mientus, R. Schieck, and S. Fiechter, *Thin Solid Films* 247, 15 (**1994**).
23. C. Guillén and J. Herrero, *Thin Solid Films* 520, 1 (**2011**).
24. M. Girtan, *Sol. Energy Mater. Sol. Cells* 100, 153 (**2012**).
25. F. Rongchuan, Solid State Spectroscopy, University of Science and Technology of China Press, HeFei (**2001**).
26. E. Ando and M. Miyazaki, *Thin Solid Films* 351, 308 (**1999**).
27. E. Ando and M. Miyazaki, *Thin Solid Films* 392, 289 (**2001**).
28. X. Jing, C. Sun, and R. J. Hong, Transparent Conductive Oxide Films, Higher Education Press, Beijing (**2008**).
29. F. Jia, X. L. Qiao, and J. G. Chen, *Chin. J. Rare Met.* 30, 505 (**2006**).
30. M. Yu, J. Zhang, D. Li, Q. Meng, and W. Li, *Surf. Coat. Technol.* 201, 1243 (**2006**).
31. Q. J. Yao, A Course in Optics, Higher Education Press, Beijing (**2002**).
32. H. S. Zhang, Half-Wave Loss and Thin Film Thickness in the Thin Film Interference, Physics Teaching in Middle School (**2001**), Vol. 30, pp. 1–2.
33. Y. P. Zhang, H. Xu, and N. Ling, *Optoelectronic Technology and Information* 19, 1 (**2006**).

Received: 5 June 2015. Accepted: 26 July 2015.